Journal of Southeast University (English Edition) Vol. 39, No. 2, pp. 176 - 186 June 2023 ISSN 1003—7985

Stepped spiral microchannels for rapid blood plasma separation

Zhang Xinjie[1,2] Zhu Hangjie[1] Liu Yao[1] Gu Qiao[3] Zhang Yuhang[1]
Oseyemi Ayobami Elisha[4] Lü Fangrui[1] Ni Zhonghua[2]

([1]College of Mechanical and Electrical Engineering, Hohai University, Changzhou 213022, China)
([2]School of Mechanical Engineering, Southeast University, Nanjing 211189, China)
([3]Department of Gynecology and Obstetrics, The Third Affiliated Hospital of Soochow University, Changzhou 213003, China)
([4]Department of Mechanical Engineering, York University, Toronto, ON M3J1P3, Canada)

Abstract: Conventional ways of blood processing, such as centrifugation and filtration, are fairly limited by processing time, separation purity, clogging, and other factors. To solve this problem, a high-throughput, inertial microfluidic device composed of a stepped spiral channel is proposed for the separation of plasma from high-concentration blood. First, the particle-focusing characteristics of the stepped spiral channel are studied through the coupling of laminar flow and particle tracking modules in the COMSOL Multiphysics® software. Next, polystyrene beads are used to investigate the inertial focusing performances of the stepped spiral channel at different flow rates. Based on the experimental results of particle focusing, an optimized stepped spiral channel is applied in blood plasma separation from samples of different cell concentrations. It can be observed that the reject ratios of the blood cells are (99.72 ± 0.13)% and (99.44 ± 0.17)% with hematocrit (HCT) values of 0.9% and 2.25%, respectively, at an optimal flow rate of 1.5 mL/min. The ratios of blood cells rejected by the stepped spiral channel are (97.02 ± 0.56)% and (92.92 ± 1.53)% at ultrahigh HCT values of 4.5% and 9%, respectively. The experimental findings demonstrate that the stepped spiral channel can efficiently separate plasma from ultrahigh-concentration blood samples.

Key words: microfluidics; inertial focusing; stepped spiral channel; blood plasma separation; secondary flow regulation
DOI: 10.3969/j.issn.1003 - 7985.2023.02.009

Blood and blood components (i.e., red blood cells (RBCs), white blood cells (WBCs), platelets, and plasma) are of utmost importance for clinical diagnostics. Blood plasma is typically used to identify the inflammatory response and potential diseases of a patient. Although conventional ways of blood processing, such as centrifugation and membrane filtration, can separate blood plasma with satisfactory efficiency, they are limited to some extent by processing time, separation purity, clogging, and other factors[1]. Centrifugation, in particular, can activate cells and affect the concentration of critical factors of analysis, such as eosinophil activity markers[2]. Microfluidic technologies provide a promising solution to overcoming the limitations of conventional methods. To date, many active and passive microfluidic technologies have been proposed for fluid and particle/cell manipulation[3-4]. Among these technologies, passive manipulation by inertial microfluidics has attracted considerable interest in the last decade owing to its simple, precise, label-free, and high-throughput operations[5-6].

The earliest report of the inertial focusing phenomenon was presented by Segré et al.[7] in 1961, which described particle focusing in terms of an annulus in a cylindrical pipe of 1 mm diameter, known as the tubular pinch effect. Subsequently, based on microfluidic technology, researchers reported a series of microchannel designs and attempted to unveil the underlying physics of inertial focusing. A straight channel is the simplest form of conduit for studying inertial focusing. Because only pure inertial forces are included in a straight channel, an overall understanding of the particle migration and focusing is possible. Many studies proved that the focusing behaviors of particles in straight channels mainly depend on channel geometry[8-9], Reynolds number (Re)[10], particle properties[11-12], and fluid properties[13]. The force balance becomes considerably complex upon inducing secondary flows in straight channels. A typical method of inducing secondary flows is using symmetric or asymmetric contraction-expansion arrays (CEAs)[14]. In a CEA channel, larger particles experience higher lift forces and are trapped by Dean vortices in the expansion region, while smaller particles follow fluid streamlines in the contraction channel; thus, particles of different sizes can be separated[15-16]. Using grooves[17-18], herringbones[19], and pillars[20-22] onto the wall surfaces can also induce strong secondary flows in straight channels, which can be used

Received 2023-01-05, **Revised** 2023-04-10.
Biography: Zhang Xinjie (1984—), male, doctor, associate professor, xj.zhang@hhu.edu.cn.
Foundation items: The National Natural Science Foundation of China (No. 51905150), Fundamental Research Funds for the Central Universities (No. B220202024), Changzhou Science and Technology Bureau Program (No. CE20225046), Changzhou Health Commission Youth Science and Technology Projects (No. QN202115), Jiangsu Planned Projects for Postdoctoral Research Funds (No. 2019K033), Postgraduate Research and Practice Innovation Program of Jiangsu Province (No. KYCX23_0670).
Citation: Zhang Xinjie, Zhu Hangjie, Liu Yao, et al. Stepped spiral microchannels for rapid blood plasma separation[J]. Journal of Southeast University (English Edition), 2023, 39(2): 176 - 186. DOI: 10.3969/j.issn.1003 - 7985.2023.02.009.

for modification of inertial focusing behavior. A universal method of inducing stable secondary flows is using curved channels. Curved channels, such as spiral[6,23-24] and asymmetric curving channels[25-27], produce a set of secondary flows in the cross-section, which effectively reduces the number of focusing bands and enhances the inertial focusing compared with straight channels.

Furthermore, the shape and strength of secondary flows can be altered by using micro-obstacle arrays, such as micropillar arrays[28] and microbar arrays[29-30], to confine flows in microchannels. By introducing a micro-obstacle array, the resulting acceleration of secondary flow can be used to enhance particle focusing. Another effective way of modifying secondary flows is to alter channel cross-section. For example, upon changing the cross-section from rectangular to trapezoidal, the asymmetry of the trapezoid modifies the shape of the velocity profile and results in the formation of strong Dean vortex cores that skew toward the wall with larger channel depth[8], resulting in higher cell separation resolution[24,31]. Other designs, such as semicircular[32], triangular[33], U-shaped[34], and combined[35] cross-sections, were also used to modify secondary flows. However, these channel designs are rarely applied due to difficulty in fabrication.

To date, many plasma separation methods have been reported by using the above-mentioned inertial microfluidic channels, such as straight channels with CEAs[2,13,15,36], serpentine channels[37], spiral channels with rectangular cross-sections[38-40], spiral channels with slanted cross-sections[1], spiral channels with ordered microbars[30], among others. These methods have undoubtedly exhibited satisfactory plasma separation efficiency. For instance, Yuan et al.[13] presented a straight channel with asymmetrical expansion-contraction cavity arrays to extract plasma from 20 × diluted blood with a viscoelastic fluid at a flow rate of 50 μL/ min. Zhang et al.[36] reported a serpentine channel to separate plasma with the same dilution ratio at a flow rate of 350 μL/min. Our group developed a spiral channel with a rectangular cross-section for plasma separation at a higher flow rate of 700 μL/ min[37]. Later, Rafeie et al.[1] used a spiral channel with a slanted cross-section to increase the blood processing throughput to 1.5 mL/min; however, their method required a whole blood dilution ratio higher than 45 ×. To separate plasma from low-dilution blood in a high-throughput manner, Shen et al.[30] proposed a spiral channel with ordered microbars to separate plasma with a dilution factor of 15 × at a flow rate of 1 to 5 mL/min. Although the past years have witnessed increased effort toward efficient plasma separation, extracting plasma from whole blood at low dilution ratios and high throughputs is still challenging.

To address the challenge, a novel inertial microfluidic device composed of a stepped spiral channel is proposed for plasma separation from high-concentration blood. First, the secondary flow and particle inertial focusing characteristics are studied by finite element simulations in the COMSOL Multiphysics® software. Next, the inertial focusing behaviors of polystyrene (PS) beads in the stepped spiral channels are studied. Finally, an optimized, stepped spiral channel is explored for plasma separation.

1 Materials and Methods

1.1 Theory of inertial focusing

In a confined straight microchannel, particles suspended in a fluid experience inertial lift and viscous drag forces. The inertial lift forces include the shear gradient lift force F_{LS}, induced by the parabolic curvature of the fluid velocity profile, and the wall lift force F_{LW}, induced by the flow field interaction between the particles and adjacent walls. For particles satisfying $a/D_h \geqslant 0.07$ (where a represents the particle diameter and D_h the hydraulic diameter of the microchannel)[25], the initial randomly dispersed particles laterally migrate to stable equilibrium positions within the channel cross-section under the influence of the net inertial lift force F_L, as the shear gradient lift force directs the particles away from the channel center and the wall lift force repels the particles away from the wall. Additionally, the particles experience the Saffman lift force $F_{L\Omega}$, which originates from particle rotation. However, $F_{L\Omega}$ is considerably weak and almost negligible in a low-aspect-ratio channel. F_L can be expressed as[41]

$$F_L = \frac{\rho U^2 a^4}{D_h^2} f_L(Re, z_C) \tag{1}$$

where ρ and U represent fluid density and maximum velocity, respectively; $f_L(Re, z_C)$ denotes a dimensionless lift coefficient and is a function of particle position within channel cross-section z_C and Reynolds number Re.

Upon introducing curvature into the rectangular channel, a secondary flow appears due to the difference in fluid speed across the cross-section, forming two symmetrical vortices known as Dean vortices. A Dean vortex induces a drag force on the particles, which regulates inertial focusing progress. Assuming a Stokes' drag, the magnitude of the Dean drag force F_D can be expressed as[42]

$$F_D = 3\pi\mu a U_D \tag{2}$$

where μ represents the fluid dynamic viscosity and U_D the average Dean velocity. Hence, the focusing performance of particles mainly depends on the balance between F_D and F_L. If F_D is equal to or weaker than F_L, the particles focus and migrate to the equilibrium positions near the inner wall.

In this study, the proposed microfluidic device includes a spiral channel of stepped cross-section, and the height

of the inner wall is considerably larger than that of the outer wall. The reason for choosing the cross-section design was to increase F_D in the inner channel in a bid to capture high-concentration blood cells near the inner wall. The stepped spiral channel could be regarded as a combination of two rectangular channels, so two pairs of independent Dean vortex cores formed in the combined channel[43]. The increased F_D induced by the inner Dean vortex cores helped to trap and focus the blood cells that could not occupy the equilibrium positions in the inner channel. Thus, plasma could be separated from the blood sample with high concentration of cells (see Fig. 1(a)).

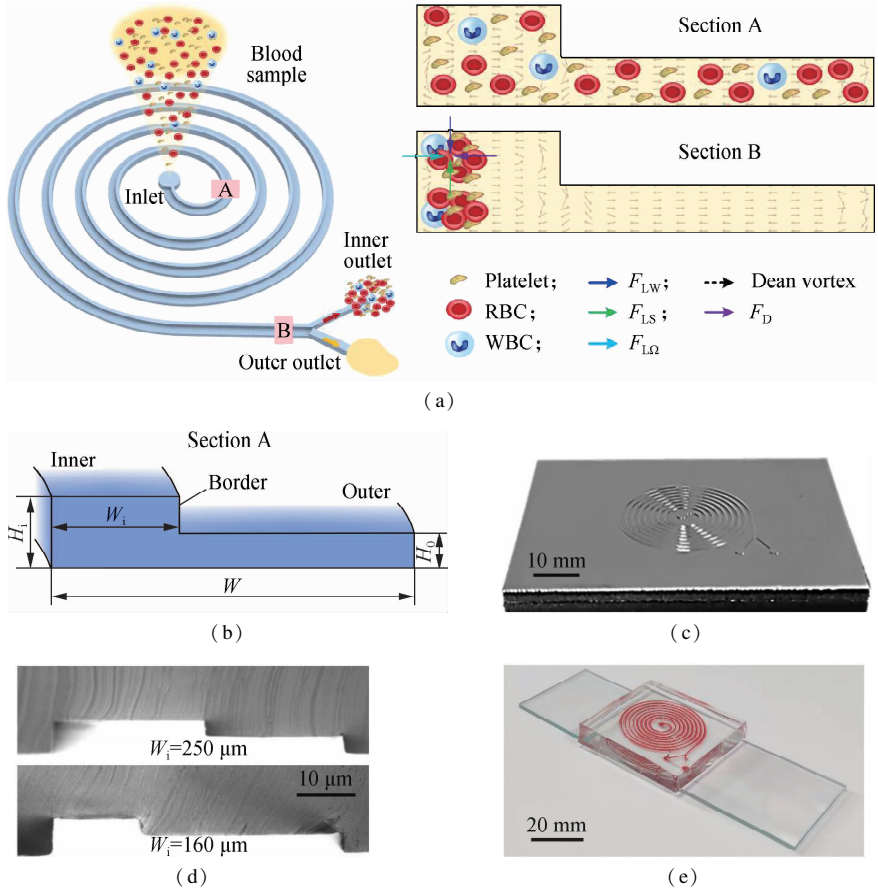

Fig. 1 Prototype of the stepped spiral channel. (a) Stepped spiral channel for blood plasma separation; (b) Cross-sectional view of the stepped spiral channel; (c) Aluminum mold; (d) Stepped cross-section; (e) Prototype device filled with red ink

1.2 Device design and fabrication

Two stepped spiral channels of different geometries were designed (see Fig. 1(b) and Tab. 1) to study the inertial focusing characteristics and determine the optimal geometry for blood plasma separation. In the cross-section of the stepped spiral channel, W and W_i represent the widths of the whole channel and inner channel, respectively, and H_i and H_o the heights of the inner wall and outer wall, respectively. The two stepped spiral channels shared a similar structure but had different values of W_i. The mold for fabricating the microfluidic device was designed in the SolidWorks® software and prepared on aluminum plates by micromilling (Beijing Jingdiao Group, Suzhou Branch) (see Fig. 1(c)). Subsequently, the device was fabricated by casting polydimethylsiloxane (PDMS, Sylgard 184 Silicone Elastomer Kit, Dow Corning) on the mold. The PDMS mixture (mass ratio of base to curing agent of 10∶1) was degassed for 20 min and baked in an oven for 2 h at 80 ℃ for curing. The cured PDMS was peeled off the mold and punched to produce fluidic inlets and outlets. Subsequently, the PDMS device was irreversibly bound to a glass slide using an oxygen plasma machine (PDC-MG, Chengdu Mingheng Science & Technology Co., Ltd., China). Finally, the assembled device was again baked in the oven at 80 ℃ for 1 h to enhance the bonding. The images of the stepped cross-section and the prototype are shown in Figs. 1(d) and (e), respectively. The measured fabrication errors of the channel height and width were about ±5 and ±12 μm, respectively.

Tab. 1 Geometric characteristics of the stepped spiral channel

Channel No.	Type (W/W_i-H_i/H_o)	W/μm	W_i/μm	H_i/μm	H_o/μm	Inner radius/μm	Gap/μm	Number of loops
1	500/250-60/30	500	250	60	30	1.5	500	8
2	500/160-60/30	500	160	60	30	1.5	500	8

1.3 Sample preparation

The focusing performance of the device was investigated using monodisperse, rigid PS beads. A total of 4 fluorescent PS microbeads with diameters of 3, 4, 6, and 10 μm (0.01 g/mL, Baseline ChromTech Research Center, Tianjin, China) were used as surrogates for platelets, RBCs, and WBCs. Beads of each size were suspended in an aqueous buffer, with a Tween 20 (0.2% volume fraction) surfactant added to form a microbead sample suspension of 0.01% volume fraction. The concentrations of the four microbead suspensions are presented in Tab. 2. We used human whole blood samples from healthy female donors for the plasma separation tests. The blood samples were diluted 2, 5, 10, 20, and 50 times with phosphate-buffered saline (PBS) for the test.

Tab. 2 Concentrations of the microbead suspensions for inertial focusing experiments

Microbead diameter/μm	Volume of deionized water/mL	Volume of microbead stock solution/mL	Concentration of microbeads/(10^6 mL^{-1})
10	20	0.2	0.17
6	20	0.2	0.82
4	20	0.2	2.80
3	20	0.2	6.60

1.4 Experimental setup

The microbead suspensions and blood samples were filled in a syringe and pumped into the microfluidic device using a syringe pump (XFP01-BD, Suzhou Xunfei Scientific Instrument Co., Ltd., China), respectively, for the inertial focusing experiment. The microfluidic device was mounted on an inverted fluorescence microscope (XDS-3, Shanghai Optical Instrument Factory No. 1, China), which was equipped with a high-speed CCD camera (Stingray F-033B/C, Allied Vision Technologies, Germany). High frame rate videos were captured at the channel outlet using the Stingray camera control software (Vimba Viewer) and then analyzed using the ImageJ® software. Furthermore, blood cell concentrations were analyzed using an automated cell counter (Countess™ 3 FL, Thermo Fisher Scientific, USA).

2 Results and Discussion

2.1 Numerical simulation of inertial focusing in the stepped spiral channel

The inertial focusing of particles in the two stepped spiral channels was investigated using the COMSOL Multiphysics® software. In the simulation, a coupled module of the Navier-Stokes equation for incompressible fluids and particle tracking was built to solve the laminar flow and inertial focusing, respectively. Water was used as the fluid material, with a density of 1 000 kg/m^3 and a dynamic viscosity of 1 g/(m · s). The discretization of fluids was set to second-order velocity and pressure, and the channel walls were defined with a no-slip boundary condition. The inlet velocities of fluid were set to 1.26 and 1.11 m/s in channel No. 1 and channel No. 2, respectively, producing the same flow rate of 1.5 mL/min. The channel outlet pressure was set to atmospheric pressure. In the particle tracing module, 15 particles with physical characteristics of 1 064 kg/m^3 density and 6 μm diameter were simultaneously dispensed at the channel entrance and set to experience the fluidic drag force and the lift force produced by the walls.

As shown in Fig. 2, the flow velocity in the inner channel was considerably higher than that in the outer one, and the randomly distributed particles in the inlet laterally migrated toward the inner channel. The secondary flow pattern is split into two pairs of Dean vortex cores in the stepped cross-section, with the stronger Dean flow in the inner channel. Because the magnitude of F_D depends on the average Dean velocity U_D, the strength of the flow velocity in the inner channel serves to influence the lateral migration of particles toward the inner wall. In channel No. 1 ($W_i = 250$ μm), 9 and 6 particles focused near the inner wall and the border at the outlet, respectively. By reducing the inner channel width to 160 μm, more particles migrated toward the inner wall again, and 13 particles focused close to the wall. The improved focusing performance of the particles observed in channel No. 2 can be explained by the theory of inertial focusing. Because the hydraulic diameter D_h of channel No. 2 is smaller than that of channel No. 1, the F_L experienced by the particles in channel No. 2 was higher than that experienced in channel No. 1. Additionally, the inner flow velocity in channel No. 2 was higher than that in channel No. 1, which produced a higher Dean drag force in channel No. 2. Therefore, most particles in channel No. 2 could focus near the wall under the higher inertial lift force and the Dean drag force.

2.2 Microbead focusing in the stepped spiral channel

Because the plasma separation was directly influenced by the focusing behavior of blood cells in the stepped spiral channel, the two microfluidic devices were tested by using fluorescent microbead suspensions. The focusing performance was characterized by evaluating the distribution and positions of the microbeads along channel width at different flow rates. The results of the study were used to identify the optimal flow rate, as well as optimize the channel design for high-efficiency blood plasma separation.

Fig. 3 shows microbead focusing in device 500/250-60/30 at a D_e of 0.73 to 13.9 (i.e., flow rates of 0.1 to 1.9 mL/min with an increment of 0.2 mL/min), and the white dashed line represents the border between the

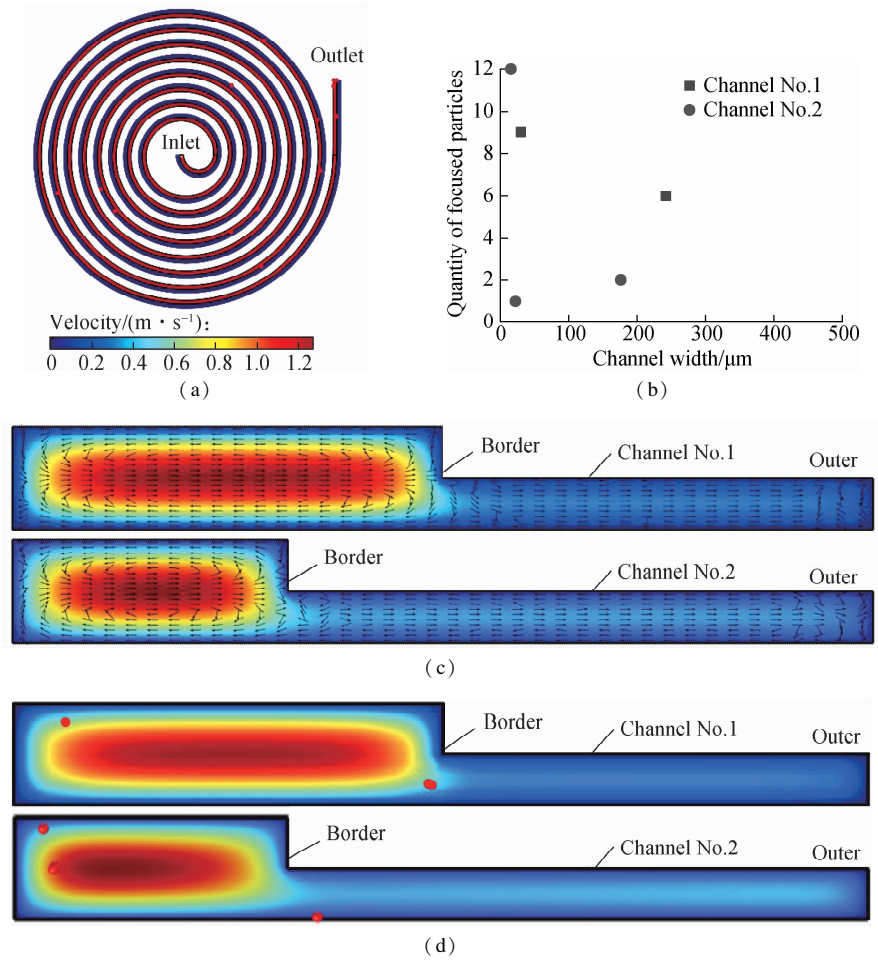

Fig. 2 Simulation results illustrating the particle focusing in the stepped spiral channels. (a) COMSOL modeling of fluid distribution and particle migration in channel No. 2; (b) Quantity of focused particles across channel width at the outlet; (c) Velocity contours of the transverse secondary flows in the stepped cross-sections; (d) Particle focusing in the stepped cross-sections

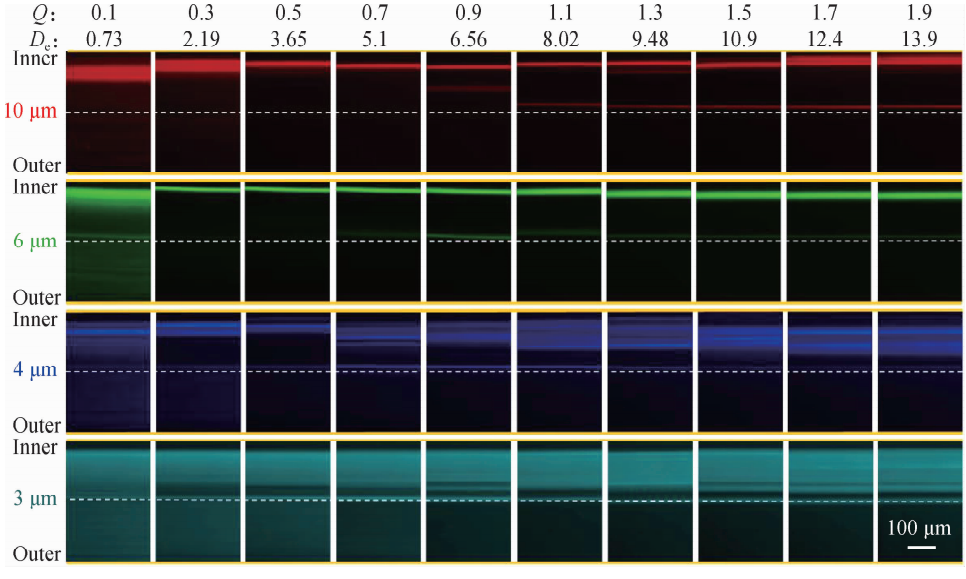

Fig. 3 Stacked fluorescent images illustrating the lateral distribution of microbeads in device 500/250-60/30

inner and outer channels. As seen from the fluorescent images, a large portion of the 10 μm microbeads focus near the inner wall even at a considerably low flow rate ($Q = 0.1$ mL/min, $D_e = 0.73$). A distinguishable single focusing band was observed near the inner wall ($Q \leqslant 0.7$ mL/min, $D_e \leqslant 5.1$) upon increasing the flow rate, which demonstrates that the microbeads experienced a dominating inertial lift force in the inner channel. A small por-

tion of the microbeads laterally migrated toward the border at higher flow rates ($Q = 0.9$ mL/min, $D_e = 6.56$). Finally, a second focusing band formed near the border ($Q \geqslant 1.3$ mL/min, $D_e \geqslant 9.48$). The focusing behavior of the 10-μm microbeads can also be explained by fluorescence intensity line scan across the channel width.

As shown in Fig. 4(a), the microbeads only exhibited a single fluorescence peak near the inner wall at D_e = 3.65. Two fluorescence peaks were observed in the inner channel upon increasing D_e to 6.56. Upon further increasing D_e from 6.56 to 13.9, the main and second peaks shifted to the inner wall and border, respectively. We can infer that at high flow rates, the increased Dean drag force gradually balanced the inertial lift force, causing the microbeads focusing near the inner wall to migrate along the equilibrium line. When a portion of the microbeads experienced a dominating Dean drag force, they left the inner wall and migrated toward the border to balance the two forces. The phenomenon of the two focusing bands in the stepped spiral channel satisfactorily verifies the findings by Rafeie et al.[35] for a spiral channel with a complex cross-section: When a complex cross-section is composed of two simple shapes, the inertial focusing in the channel is a combination of particle behaviors in each channel. Accordingly, because the stepped spiral channel can be divided into two spiral channels with rectangular cross-sections that have a single focusing position each, the two focusing positions in the stepped spiral channel can be considered to be a combination of the focusing effects of the two rectangular channels.

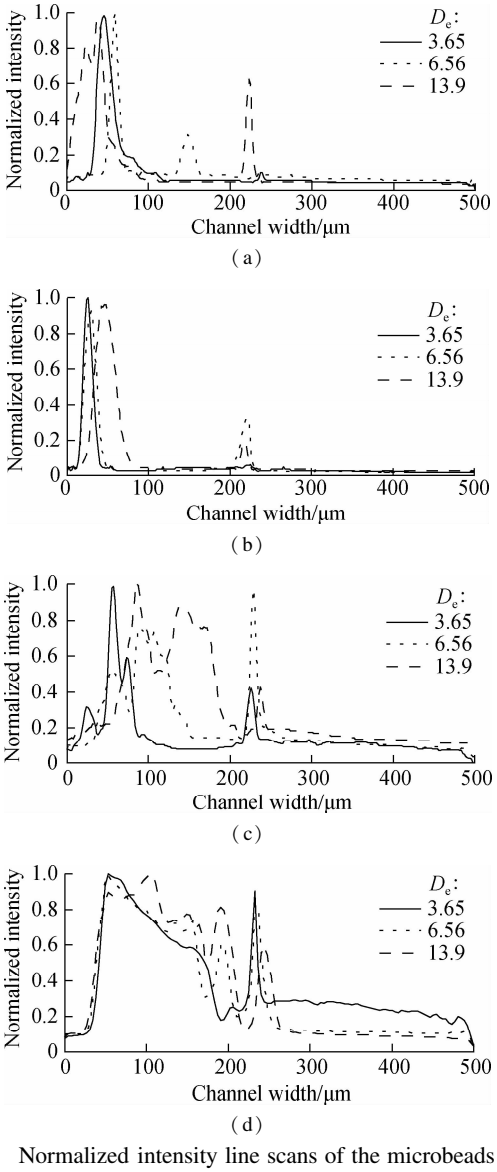

Fig. 4 Normalized intensity line scans of the microbeads in device 500/250-60/30. (a) 10 μm microbeads; (b) 6 μm microbeads; (c) 4 μm microbeads; (d) 3 μm microbeads

The focusing performance of the 6 μm microbeads was fairly similar to that of the 10 μm ones. However, the fluorescent intensity of the second focusing band was considerably weaker than the first band, which means that most microbeads focused to the main peak (see Fig. 4(b)). Upon testing the 4 μm microbeads, they initially dispersed in the channel. However, by increasing D_e, the microbeads could focus into a relatively narrow band, which occupied approximately half of the lateral width of the inner channel (see Fig. 4(c)). Additionally, a second peak of the microbeads formed near the border at D_e higher than 5.1. The 3 μm microbeads could not realize tight focusing due to the influence of a weaker inertial lift force. However, most 3 μm microbeads could be trapped in the inner channel (see Fig. 4(d)). We can conclude that the rough focusing of the 3 μm microbeads was caused by the dominating Dean vortex in the inner channel. The microbeads were trapped in the inner channel to follow the strong, counter-rotation Dean vortex because the inertial lift force was weaker than the Dean drag force.

Because device 500/250-60/30 had two inertial focusing positions in the inner channel and the position of the second band was close to the inner border, it is indicated that the focusing band was influenced by the lateral position of the border across channel width. The width of the inner channel was decreased to 160 μm to investigate the effect of border position on particle focusing. This geometry optimization was intended to decrease the Dean drag force in the outer channel and eliminate the second focusing band. The focusing performance of the microbeads in the optimized channel is shown in Fig. 5. As expected, the 10, 6, and 4 μm microbeads tightly focused near the inner wall at D_e higher than 2.5 (flow rate $Q \geqslant 0.5$ mL/min), while the 3 μm ones roughly focused into a wide band in the inner channel at D_e higher than 4.5 (flow rate $Q \geqslant 0.9$ mL/min). Moreover, all the microbeads had only a single focusing band in the inner channel.

Fig. 6 shows the normalized intensity line scans of microbeads in the two channels at a D_e of 7.5 (flow rate of 1.5 mL/min). In comparison with the first device (W_i = 250 μm), the fluorescent intensity lines of the microbeads

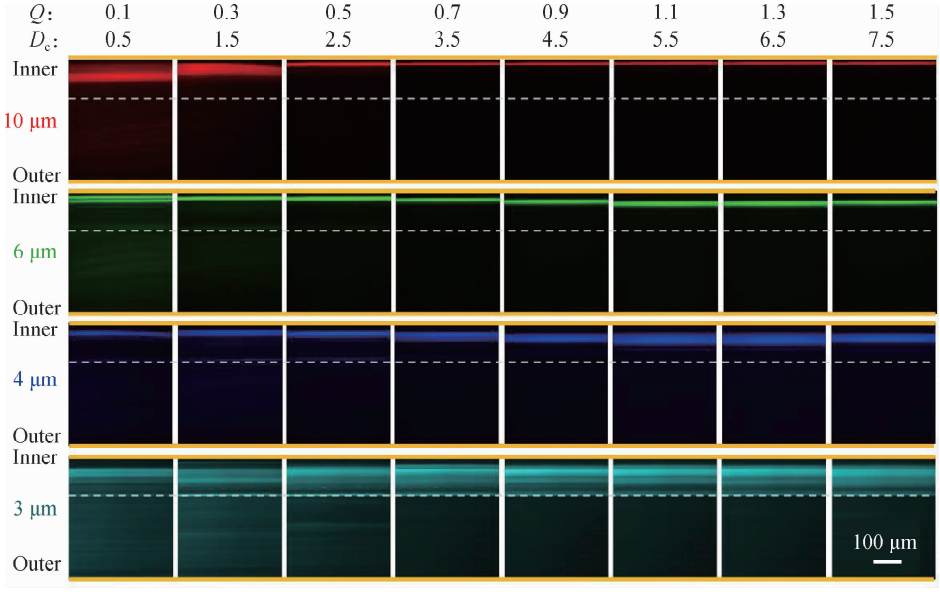

Fig. 5 Stacked fluorescent images illustrating the lateral distribution of the microbeads in device 500/160-60/30

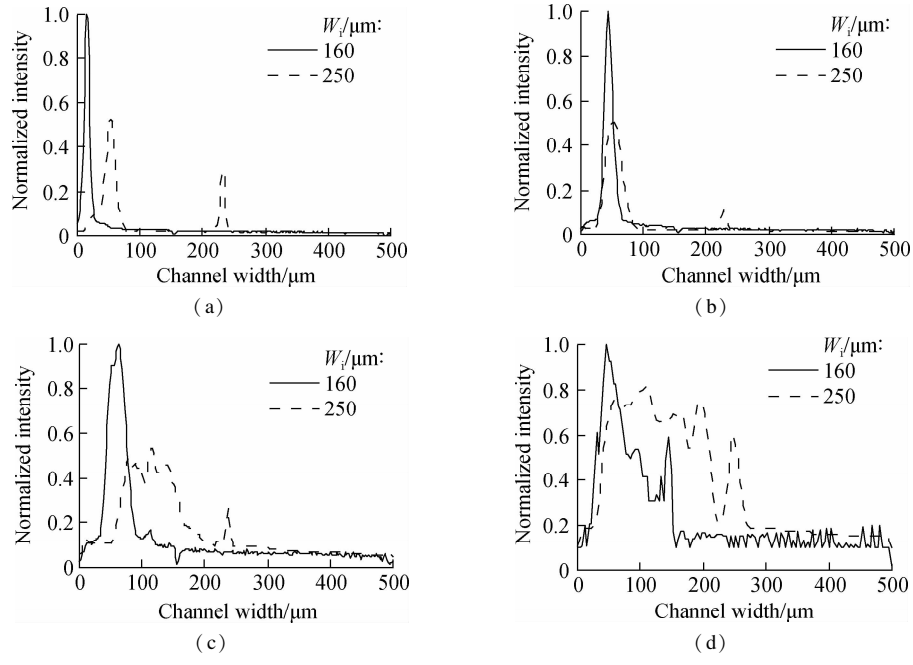

Fig. 6 Comparisons of normalized intensity line scans of the microbeads in the two stepped spiral channels. (a) 10 μm microbeads; (b) 6 μm microbeads; (c) 4 μm microbeads; (d) 3 μm microbeads

in the optimized device ($W_i = 160$ μm) were apparently skewed toward the inner channel, with the fluorescent peaks being considerably higher, which demonstrates the better focusing efficiency of the optimized device. The experimental results satisfactorily verify that the focusing behavior (i.e., position and quantity of focusing band) of microbeads can be altered by changing the lateral border position of the stepped spiral channel. These findings satisfactorily supplement the current knowledge of the physics of particles focusing in complex channels. Additionally, the hydraulic diameter of the stepped channel in the first device was $D_h = 4A/P = 72.66$ μm (where A is the cross-sectional area of the stepped channel, P is the wetted perimeter of the cross-section.), requiring the particle size to be at least 5.09 μm to meet the classic focusing criterion (i.e., $a/D_h \geqslant 0.07$). However, the optimized channel could tightly focus the 4 μm microbeads, and even the 3 μm ones could be successfully trapped in the inner channel, which refuted the focusing criterion. Therefore, the stepped spiral channel exhibited a better focusing effect than a regular channel with a rectangular cross-section, which should earnestly obey the classic focusing criterion.

Upon analyzing the fluorescent focusing positions of the microbeads, we observed that flow rates higher than 0.9 mL/min were appropriate for single band focusing in

the inner channel of device 500/160-60/30, which would also be applicable for blood plasma separation. However, because some microbeads distributed in the outer channel may not be visible due to the overwhelming fluorescent intensity of the focusing bands in the inner channel, the focusing behavior of the microbeads in the fluorescent images is not sufficient to determine the optimal flow rate for high-efficiency plasma separation. The focusing behaviors of all the microbeads were examined in a bright field to determine the optimal flow rate with minimum microbeads in the outer channel. As shown in Fig. 7, all 10, 6, and 4 μm microbeads focused in the inner channel at flow rates higher than 0.7, 1.1, and 1.3 mL/min, respectively, while the least number of the 3 μm microbeads were distributed in the outer channel at flow rates higher than 1.1 mL/min. Therefore, the flow rate of 1.5 mL/min was selected for blood plasma separation in the optimized device.

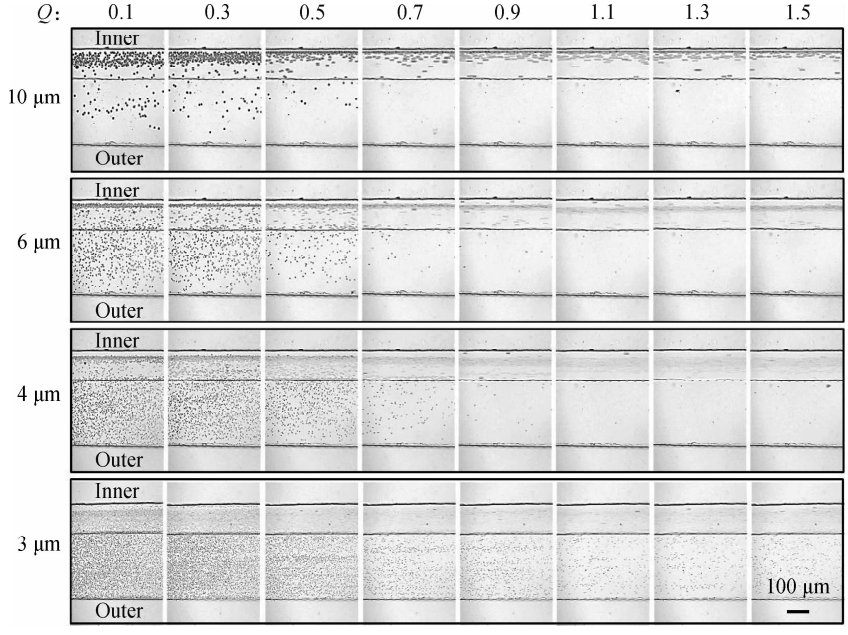

Fig. 7 Stacked bright images of the 10, 6, 4, and 3 μm microbeads focusing in the stepped spiral channel of device 500/160-60/30

2.3 Characterization of blood plasma separation

In the plasma separation test, human whole blood was diluted by 2, 5, 10, 20, and 50 times with PBS, with the corresponding hematocrit (HCT) values of 22.5%, 9%, 4.5%, 2.25%, and 0.9%, respectively. The blood plasma separation performances at different HCT values are shown in Fig. 8. As shown in the 0.9% HCT experiment, the blood cells focused into a band near the inner wall, which is similar to the focusing behavior of the PS beads. Because all the blood cells focused in the inner channel, the plasma collected from the outer outlet was totally transparent, and only several blood cells were observed in the collected plasma. The focusing positions of the blood cells remained the same for all the blood samples upon increasing the HCT value. However, the focusing band of the blood cells widened due to intensive interactions between the high-concentration cells, causing a small portion of the cells (in the cases of 4.5% and 9% HCT) to leave the focusing position and distribute to the outer channel. Therefore, more blood cells were observed in the collected plasma, and the plasma in the centrifugal tube was visually red.

Fig. 9(a) shows the bright field intensity profile along the channel width. Because the gray values of black and

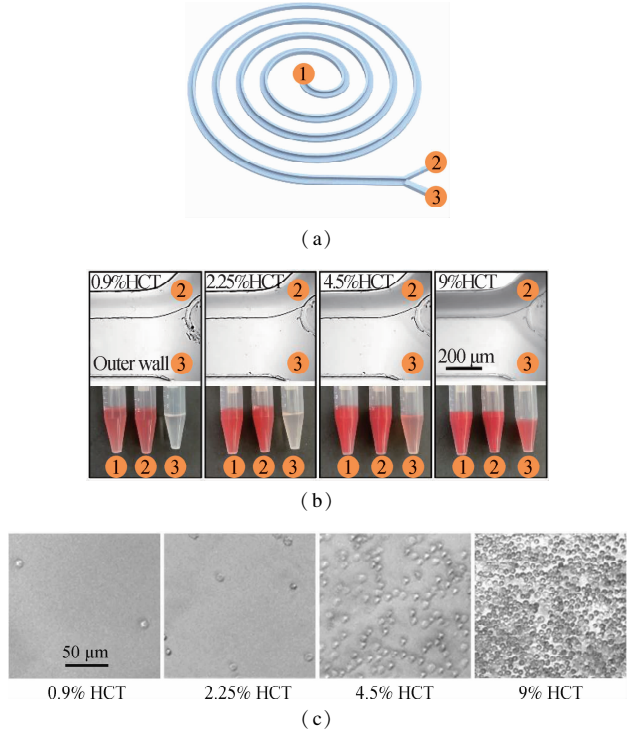

Fig. 8 Blood plasma separation performances at different HCT values. (a) The stepped spiral channel; (b) Plasma separation and corresponding suspensions collected from different outlets; (c) Residual blood cells in the collected plasma

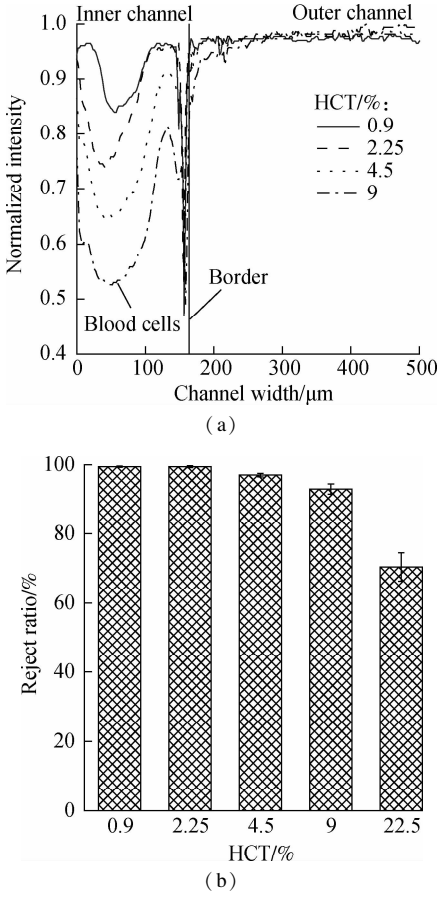

Fig. 9 Quantitative analysis of blood plasma separation at different HCT values. (a) Bright field intensity profile illustrating the blood cell focusing position along channel width; (b) Reject ratio of blood cells in the separation process

white colors were set to 0 and 255, respectively, by the ImageJ® software, the blood cells (i.e., dark stream in the inner channel in Fig. 8(b)) had considerably lower intensity than the outer channel (i.e., white background in Fig. 8(b)). Therefore, the lower the intensity, the more cells that occupy the bright field. The profile width and depth of the blood cell focusing band widened and deepened upon increasing HCT, which means more blood cells were captured in the inner channel. To quantitatively study the separation efficiency, the collected blood plasma was placed in an automated cell counter to examine the blood cell concentration value. The obtained concentration was used to calculate the reject ratio of the blood cells, which could be used to reflect the separation efficiency. Here the reject ratio can be expressed as $1 - C_p/C_i$, where C_p represents the number of blood cells in collected plasma and C_i the number of the blood cells in the input blood sample. As shown in Fig. 9(b), (99.72 ± 0.13)% of blood cells were removed during the inertial separation process at an HCT value of 0.9%. The device still maintained a high reject ratio of (99.44 ± 0.17)% upon increasing the HCT value to 2.25%. The reject ratio gradually decreased due to the pollution of blood cells entering the outer channel when the HCT value was increased to 4.5% and 9%. By increasing HCT to an ultra-high value of 22.5%, the inner channel was filled with intensive blood cells, forcing the overloading cells to the outer channel. In this scenario, the reject ratio sharply decreased to (70.46 ± 4.13)%. Thus, high-purity plasma cannot be obtained at higher HCT values. We further compared the blood plasma separation performances of the device with the performances of reported inertial microfluidic devices[1-2,13,15,30,36-40]. For the diluted blood with an HCT value below 2.25%, our device achieved comparable blood plasma separation efficiency and the highest processing throughput (33.33 and 75 μL/min at 0.9% and 2.25% HCT values, respectively; the equivalent flow rate of whole blood for a single channel) among those devices. The yield of plasma was about 573.53 μL/min. For the HCT value above 4.5%, most devices could not be used for high-efficiency plasma separation, and no device could separate plasma at HCT values above 9%. Our device could successfully separate plasma at high HCT values, and the purity of the separated plasma was (97.02 ± 0.56)% and (92.92 ± 1.53)% at 4.5% and 9% HCT values, respectively. The experimental results demonstrate that our device with a stepped spiral channel exhibits remarkable plasma separation performance, particularly when HCT values are high. Therefore, the proposed device can be considered applicable for high-throughput plasma separation from high-concentration blood samples with less dilution.

3 Conclusions

1) We developed an inertial microfluidic device with a stepped spiral channel for rapid blood plasma separation. The inertial focusing performance of the stepped spiral channel was studied through coupled simulations of laminar flow and particle tracing in the COMSOL Multiphysics® software and experiments using fluorescent PS beads of four different diameters at various flow rates.

2) The experimental results demonstrated that two focusing bands of the microbeads could be formed near the inner wall and border and that a solely tight focusing band could also be formed by altering the border position of the stepped spiral channel. The optimal channel was then applied for blood plasma separation at an optimal flow rate of 1.5 mL/min, following which plasma separation efficiencies at different HCT values were investigated. We observed that the reject ratios of blood cells in the stepped spiral channel were (99.72 ± 0.13)% and (99.44 ± 0.17)% at HCT values of 0.9% and 2.25%, respectively. Additionally, (97.02 ± 0.56)% and (92.92 ± 1.53)% of blood cells were rejected for higher HCT values of 4.5% and 9%, respectively.

3) The stepped spiral channel exhibited remarkable plasma separation efficiency, particularly for a high-concentration blood sample. Overall, the inertial microfluidic

technology is expected to significantly benefit from enhanced microchannels with complex geometries, which will further improve the efficiency of manipulation of microparticles and cells.

References

[1] Rafeie M, Zhang J, Asadnia M, et al. Multiplexing slanted spiral microchannels for ultra-fast blood plasma separation[J]. *Lab on a Chip*, 2016, **16**(15): 2791 - 2802. DOI: 10.1039/C6LC00713A.

[2] Lee M G, Shin J H, Choi S, et al. Enhanced blood plasma separation by modulation of inertial lift force[J]. *Sensors and Actuators B: Chemical*, 2014, **190**: 311 - 317. DOI: 10.1016/j.snb.2013.08.092.

[3] Farahinia A, Zhang W J, Badea I. Novel microfluidic approaches to circulating tumor cell separation and sorting of blood cells: A review[J]. *Journal of Science: Advanced Materials and Devices*, 2021, **6**(3): 303 - 320. DOI: 10.1016/j.jsamd.2021.03.005.

[4] Tang W L, Zhu S, Jiang D, et al. Channel innovations for inertial microfluidics[J]. *Lab on a Chip*, 2020, **20**(19): 3485 - 3502. DOI: 10.1039/d0lc00714e.

[5] Zhang X J, Zhu Z X, Xiang N, et al. Automated microfluidic instrument for label-free and high-throughput cell separation[J]. *Analytical Chemistry*, 2018, **90**(6): 4212 - 4220. DOI: 10.1021/acs.analchem.8b00539.

[6] Xiang N, Ni Z H. High-throughput concentration of rare malignant tumor cells from large-volume effusions by multistage inertial microfluidics[J]. *Lab on a Chip*, 2022, **22**(4): 757 - 767. DOI: 10.1039/d1lc00944c.

[7] Segré G, Silberberg A. Radial particle displacements in poiseuille flow of suspensions[J]. *Nature*, 1961, **189**(4760): 209 - 210. DOI: 10.1038/189209a0.

[8] Moloudi R, Oh S, Yang C, et al. Inertial particle focusing dynamics in a trapezoidal straight microchannel: Application to particle filtration[J]. *Microfluidics and Nanofluidics*, 2018, **22**(3): 33. DOI: 10.1007/s10404-018-2045-5.

[9] Wang X, Zandi M, Ho C C, et al. Single stream inertial focusing in a straight microchannel[J]. *Lab on a Chip*, 2015, **15**(8): 1812 - 1821. DOI: 10.1039/c4lc01462f.

[10] Liu C, Hu G Q, Jiang X Y, et al. Inertial focusing of spherical particles in rectangular microchannels over a wide range of Reynolds numbers[J]. *Lab on a Chip*, 2015, **15**(4): 1168 - 1177. DOI: 10.1039/C4LC01216J.

[11] Hur S C, Henderson-MacLennan N K, McCabe E R B, et al. Deformability-based cell classification and enrichment using inertial microfluidics[J]. *Lab on a Chip*, 2011, **11**(5): 912 - 920. DOI: 10.1039/C0LC00595A.

[12] Hur S C, Choi S E, Kwon S, et al. Inertial focusing of non-spherical microparticles[J]. *Applied Physics Letters*, 2011, **99**(4): 044101. DOI: 10.1063/1.3608115.

[13] Yuan D, Zhang J, Sluyter R, et al. Continuous plasma extraction under viscoelastic fluid in a straight channel with asymmetrical expansion-contraction cavity arrays[J]. *Lab on a Chip*, 2016, **16**(20): 3919 - 3928. DOI: 10.1039/C6LC00843G.

[14] Jiang D, Huang D, Zhao G T, et al. Numerical simulation of particle migration in different contraction-expansion ratio microchannels[J]. *Microfluidics and Nanofluidics*, 2019, **23**(1): 7. DOI: 10.1007/s10404-018-2176-8.

[15] Lee M G, Choi S, Kim H J, et al. Inertial blood plasma separation in a contraction-expansion array microchannel[J]. *Applied Physics Letters*, 2011, **98**(25): 253702. DOI: 10.1063/1.3601745.

[16] Bhagat A A S, Hou H W, Li L D, et al. Pinched flow coupled shear-modulated inertial microfluidics for high-throughput rare blood cell separation[J]. *Lab on a Chip*, 2011, **11**(11): 1870 - 1878. DOI: 10.1039/C0LC00633E.

[17] Choi S, Karp J M, Karnik R. Cell sorting by deterministic cell rolling[J]. *Lab on a Chip*, 2012, **12**(8): 1427 - 1430. DOI: 10.1039/C2LC21225K.

[18] Golden J P, Kim J S, Erickson J S, et al. Multi-wavelength microflow cytometer using groove-generated sheath flow[J]. *Lab on a Chip*, 2009, **9**(13): 1942 - 1950. DOI: 10.1039/B822442K.

[19] Stroock A D, Dertinger S K W, Ajdari A, et al. Chaotic mixer for microchannels[J]. *Science*, 2002, **295**(5555): 647 - 651. DOI: 10.1126/science.1066238.

[20] Stoecklein D, Wu C Y, Kim D, et al. Optimization of micropillar sequences for fluid flow sculpting[J]. *Physics of Fluids*, 2016, **28**(1): 012003.

[21] Amini H, Sollier E, Masaeli M, et al. Engineering fluid flow using sequenced microstructures[J]. *Nature Communications*, 2013, **4**: 1826. DOI: 10.1038/ncomms2841.

[22] Paulsen K S, Chung A J. Non-spherical particle generation from 4D optofluidic fabrication[J]. *Lab on a Chip*, 2016, **16**(16): 2987 - 2995. DOI: 10.1039/C6LC00208K.

[23] Hou H W, Warkiani M E, Khoo B L, et al. Isolation and retrieval of circulating tumor cells using centrifugal forces[J]. *Scientific Reports*, 2013, **3**: 1259. DOI: 10.1038/srep01259.

[24] Zhu Z X, Wu D, Li S, et al. A polymer-film inertial microfluidic sorter fabricated by jigsaw puzzle method for precise size-based cell separation[J]. *Analytica Chimica Acta*, 2021, **1143**: 306 - 314. DOI: 10.1016/j.aca.2020.11.001.

[25] Di Carlo D, Irimia D, Tompkins R G, et al. Continuous inertial focusing, ordering, and separation of particles in microchannels[J]. *Proceedings of the National Academy of Sciences of the United States of America*, 2007, **104**(48): 18892 - 18897. DOI: 10.1073/pnas.0704958104.

[26] Zhang Y, Zhang J, Tang F, et al. Design of a single-layer microchannel for continuous sheathless single-stream particle inertial focusing[J]. *Analytical Chemistry*, 2018, **90**(3): 1786 - 1794. DOI: 10.1021/acs.analchem.7b03756.

[27] Zhang J, Li W H, Li M, et al. Particle inertial focusing and its mechanism in a serpentine microchannel[J]. *Microfluidics and Nanofluidics*, 2014, **17**(2): 305 - 316. DOI: 10.1007/s10404-013-1306-6.

[28] Geng Z X, Ju Y R, Wang W, et al. Continuous blood separation utilizing spiral filtration microchannel with gradually varied width and micro-pillar array[J]. *Sensors*

and Actuators B: *Chemical*, 2013, **180**: 122 - 129. DOI: 10.1016/j.snb.2012.06.064.

[29] Shen S F, Tian C, Li T B, et al. Spiral microchannel with ordered micro-obstacles for continuous and highly-efficient particle separation[J]. *Lab on a Chip*, 2017, **17**(21): 3578 - 3591. DOI: 10.1039/C7LC00691H.

[30] Shen S F, Zhang F J, Wang S T, et al. Ultra-low aspect ratio spiral microchannel with ordered micro-bars for flow-rate insensitive blood plasma extraction[J]. *Sensors and Actuators B*: *Chemical*, 2019, **287**: 320 - 328. DOI: 10.1016/j.snb.2019.02.066.

[31] Warkiani M E, Guan G F, Luan K B, et al. Slanted spiral microfluidics for the ultra-fast, label-free isolation of circulating tumor cells[J]. *Lab on a Chip*, 2014, **14**(1): 128 - 137. DOI: 10.1039/C3LC50617G.

[32] Kim J, Lee J, Wu C, et al. Inertial focusing in non-rectangular cross-section microchannels and manipulation of accessible focusing positions[J]. *Lab on a Chip*, 2016, **16**(6): 992 - 1001. DOI: 10.1039/C5LC01100K.

[33] Chen Z Z, Zhao L, Wei L J, et al. River meander-inspired cross-section in 3D-printed helical microchannels for inertial focusing and enrichment[J]. *Sensors and Actuators B*: *Chemical*, 2019, **301**: 127125. DOI: 10.1016/j.snb.2019.127125.

[34] Mehran A, Rostami P, Saidi M S, et al. High-throughput, label-free isolation of white blood cells from whole blood using parallel spiral microchannels with U-shaped cross-section[J]. *Biosensors*, 2021, **11**(11): 406. DOI: 10.3390/bios11110406.

[35] Rafeie M, Hosseinzadeh S, Taylor R A, et al. New insights into the physics of inertial microfluidics in curved microchannels. Ⅰ. Relaxing the fixed inflection point assumption[J]. *Biomicrofluidics*, 2019, **13**(3): 034117. DOI: 10.1063/1.5109004.

[36] Zhang J, Yan S, Li W H, et al. High throughput extraction of plasma using a secondary flow-aided inertial microfluidic device[J]. *RSC Advances*, 2014, **4**(63): 33149 - 33159. DOI: 10.1039/C4RA06513A.

[37] Xiang N, Ni Z H. High-throughput blood cell focusing and plasma isolation using spiral inertial microfluidic devices[J]. *Biomedical Microdevices*, 2015, **17**(6): 110. DOI: 10.1007/s10544-015-0018-y.

[38] Mach A J, Di Carlo D. Continuous scalable blood filtration device using inertial microfluidics[J]. *Biotechnology and Bioengineering*, 2010, **107**(2): 302 - 311. DOI: 10.1002/bit.22833.

[39] Robinson M, Marks H, Hinsdale T, et al. Rapid isolation of blood plasma using a cascaded inertial microfluidic device[J]. *Biomicrofluidics*, 2017, **11**(2): 024109. DOI: 10.1063/1.4979198.

[40] Han J Y, DeVoe D L. Plasma isolation in a syringe by conformal integration of inertial microfluidics[J]. *Annals of Biomedical Engineering*, 2021, **49**(1): 139 - 148. DOI: 10.1007/s10439-020-02526-9.

[41] Di Carlo D. Inertial microfluidics[J]. *Lab on a Chip*, 2009, **9**(21): 3038 - 3046.

[42] Kuntaegowdanahalli S S, Bhagat A A S, Kumar G, et al. Inertial microfluidics for continuous particle separation in spiral microchannels[J]. *Lab on a Chip*, 2009, **9**(20): 2973 - 2980. DOI: 10.1039/B908271A. [LinkOut]

[43] Han S, Zhang X J, Gu Q, et al. Inertial focusing effect of particles in spiral microchannel with asymmetric cross-section[J]. *Optics and Precision Engineering*, 2022, **30**(3): 310 - 319. DOI: 10.37188/OPE.20223003.0310. (in Chinese)

用于快速分离血浆的阶梯型螺旋微流道

张鑫杰[1,2] 朱行杰[1] 刘 尧[1] 顾 乔[3] 张宇航[1]
Oseyemi Ayobami Elisha[4] 吕芳蕊[1] 倪中华[2]
([1] 河海大学机电工程学院, 常州 213022)
([2] 东南大学机械工程学院, 南京 211189)
([3] 苏州大学附属第三医院妇产科, 常州 213003)
([4]Department of Mechanical Engineering, York University, Toronto, ON M3J1P3, Canada)

摘要:为解决传统血液处理方法如离心和过滤等存在处理时间、分离纯度、堵塞性等方面限制的问题,设计一种高通量惯性微流控芯片,该芯片由阶梯型螺旋流道组成,可用于高浓度血浆分离. 首先,采用 COMSOL Multiphysics®软件的层流和粒子追踪模块仿真研究阶梯型螺旋流道中粒子的聚焦特性. 然后,通过实验研究了不同流量下聚苯乙烯粒子在流道中的惯性聚焦行为. 最后,基于粒子聚焦实验结果,选择了一种优化结构的阶梯型螺旋流道,以用于不同浓度血液中血浆的分离应用. 实验发现,在最优流量 1.5 mL/min 时,血细胞容积为 0.9% 和 2.25% 的血样中血细胞移除率分别达到(99.72 ± 0.13)% 和(99.44 ± 0.17)%. 当血细胞容积高达 4.5% 和 9.0% 时,该阶梯型螺旋流道仍然具有(97.02 ± 0.56)% 和(92.92 ± 1.53)% 的血细胞移除率. 实验结果表明,阶梯型螺旋流道可以从高浓度血样中高效分离血浆.

关键词:微流控;惯性聚焦;阶梯型螺旋流道;血浆分离;二次流调控
中图分类号:TH77